MAPPING FOREST VEGETATION WITH ERTS-1 MSS DATA AND AUTOMATIC DATA PROCESSING TECHNIQUES

J. Messmore*, G. E. Copeland† and G. F. Levy∆

Department of Biology
and Department of Physics and Geophysical Sciences
Old Dominion University, Norfolk, Virginia

Abstract

This study was undertaken with the intent of elucidating the forest mapping capabilities of ERTS-1 MSS data when analyzed with the aid of LARS' automatic data processing techniques. The site for this investigation was the Great Dismal Swamp, a 210,000 acre wilderness area located on the Middle Atlantic coastal plain. Due to inadequate ground truth information on the distribution of vegetation within the swamp, an unsupervised classification scheme was utilized. Initially pictureprints, resembling low resolution photographs, were generated in each of the four ERTS-1 channels. Data found within rectangular training fields was then clustered into 13 spectral groups and defined statistically. Using a maximum likelihood classification scheme, the unknown data points were subsequently classified into one of the designated training classes. Training field data was classified with a high degree of accuracy (greater than 95%), and progress is being made towards identifying the mapped spectral classes.

---

* Graduate Student, Department of Biology
† Assistant Professor, Department of Physics and Geophysical Sciences
∆ Associate Professor, Department of Biology

(NASA-CR-148136) MAPPING FOREST VEGETATION WITH ERTS-1 MSS DATA AND AUTOMATIC DATA PROCESSING TECHNIQUES (Old Dominion Univ., Norfolk, Va.) 18 p HC $3.50 CSCL 08B

N76-24680

Unclas
G3/43 28345

J. Messmore, G. E. Copeland and G. F. Levy

Introduction

A great impetus to the field of remote sensing was realized in July of 1972 with the launch of the Earth Resources Technology Satellite (ERTS-1; now designated LANDSAT-1). Since that date, large quantities of digital imagery have been generated, though the applicability of this satellite data to specific problems remains to be fully investigated.

Computer-aided analysis of ERTS-1 data, as applied to forest mapping, has not been extensively investigated and comparatively little has been published on this phase of satellite data application. However, Erb (1973) utilized ERTS-1 data to detect, identify, and measure forest and agricultural features of interest. In addition, Heath and Parker (1973) used automatic computer processing techniques to map timber stands and range plants in the Houston, Texas area.

This study examines the feasibility of applying ERTS-1 MSS data and automatic data processing techniques as a means of mapping forest vegetation. The site for this investigation is the Great Dismal Swamp, a 210,000 acre forested area which transects the Virginia-North Carolina border. This region is of special interest, as it is one of the last large wilderness areas remaining along the Middle Atlantic coastal plain (Fig. 1). Due to its unique geographic location, both northern and southern flora can be found growing there. Meanly (1973) characterized the Great Dismal Swamp's vegetation as having five major plant communities: 1) Hydric or deep water swamp, 2) Semihydric or mixed swamp forest, 3) Mesic forest, 4) Atlantic white cedar forest, 5) Evergreen shrub bog or pocosin. To date, application of ERTS-1 data to specific studies within the swamp is limited to the hydrologic and vegetational investigations of Carter in 1974.

Being the wilderness it is, the Great Dismal Swamp lends itself well to remote sensing studies. Many interior regions are largely inaccessible to ground survey and, consequently, little is known about these areas. Through the use of remotely sensed data, such as ERTS-1, the need for large amounts of expensive and time consuming ground-obtained data can be minimized.

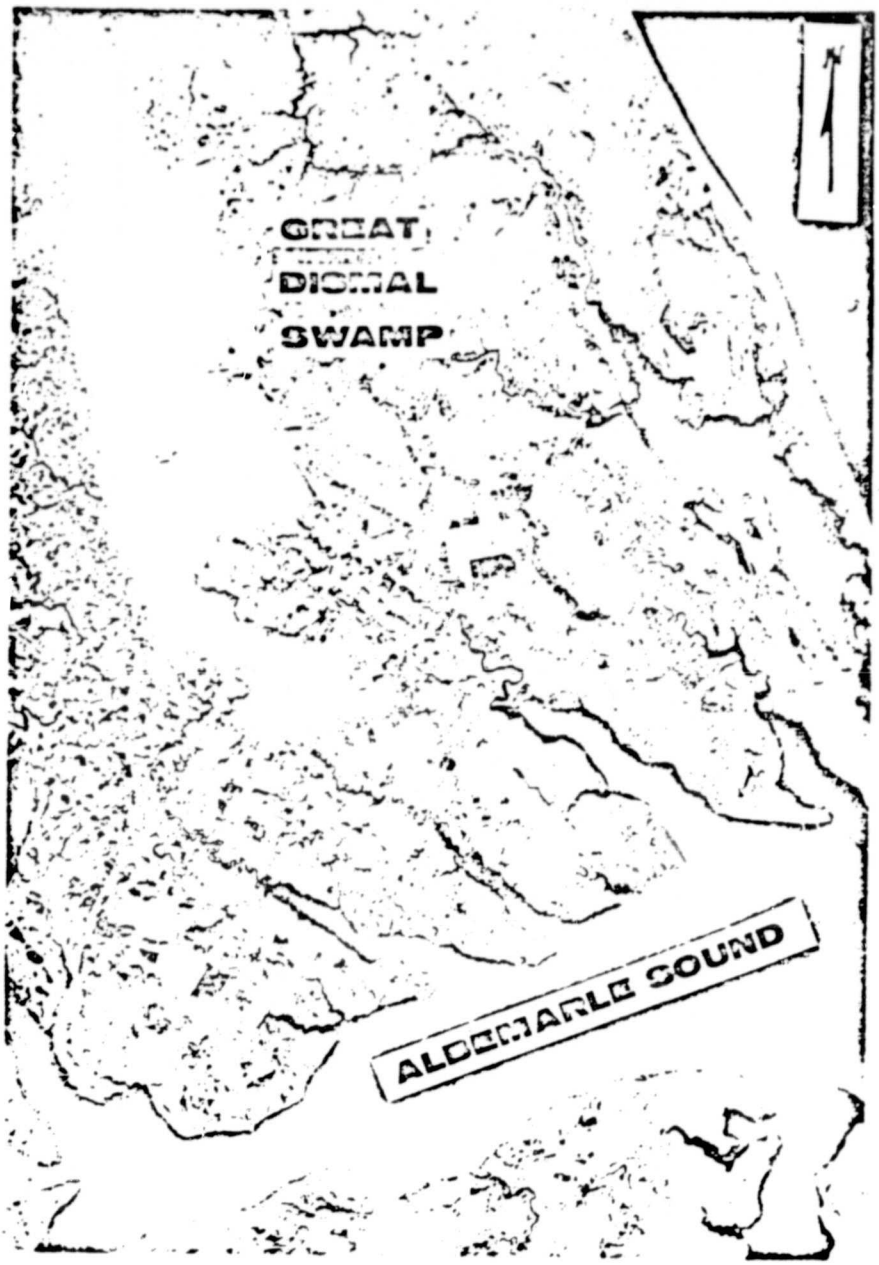

Fig. 1 A portion of ERTS image No. 1205-15150 (MSS 5) acquired on Feb. 13, 1973. (In the current study, August data was utilized.)

J. Messmore, G. E. Copeland, and G. F. Levy

Materials and Methods

On August 30, 1973, ERTS-1 remotely acquired data of an area 100 x 100 nautical miles on the eastern coast of the United States. Contained within this MSS data was the study site of this investigation, the Great Dismal Swamp (See Figure 1). Analysis of the spectral data obtained over the swamp was accomplished through the use of automatic data processing techniques developed by the Laboratory for Applications of Remote Sensing at Purdue University. Access to these ADP techniques was provided by a remote computer terminal located at the NASA Langley Research Center, Hampton, Virginia.

Generally, an unsupervised classification scheme, such as applied in this research, begins by defining as training fields those areas within the study site that contain representative vegetative cover. This information is then divided into "X" number of clusters based on the distribution of spectral information within the training field data. The reflectivity of each cluster or spectral class is then defined in terms of its mean vector and covariance matrix. The data points representing unknown ground features within the area to be mapped are subsequently classified into one of the user-defined spectral classes by a pattern recognition algorithm. Final analysis centers upon determination of the relationship between the mapped spectral classes and known surface data, i.e., ground truth comparison.

Pictureprint. The first computer program to be run in this study was the picture-print function. This program produces a gray scale printout of the digital data from one channel of the ERTS multispectral scanner. Various shades of gray are represented by specific alphanumeric symbols. These are assigned so that highly reflective areas are represented by a symbol which covers a low percentage of the printout, such as . . . ; absorbent terrain is differentiated from other areas by assigning a dense appearing symbol, e.g., BBBB. Because spectral information representing ground terrain will not be evenly distributed between the highest and lowest reflectance values, the data is histogrammed. Symbols are then assigned to radiance values such that each has approximately the same probability of being printed. As an interpretive tool, the pictureprint can be very useful in developing a grasp of the data's spatial orientation and in locating areas of known composition.

Cluster. After designating training areas to the

computer, the cluster function is run. This program is necessary because the pattern recognition algorithm assumes that each spectral class can be characterized by a multidimensional Gaussian density function. The dimensionality of this space is the number of distinct spectral bands present in the imagery (ERTS-1 has 4 bands). Clustering the training data gives an indication of whether or not the data tends to be Gaussian and provides a means for dividing it into approximate Gaussian sub-classes if the original data is non-Gaussian (Lindenlaub, 1973). Options available within the cluster function allow the researcher to choose any combination of available spectral bands, as well as the number of cluster groups to be separated within the data. The cluster function output, in addition to providing maps of the clustered data, also provides a listing of the pairwise separability values. This information is useful in determining the uniqueness of spectral clusters within the training field data.

Statistics. This processing function provides an estimate of each training classes' mean vector and covariance matrix. These statistics are usually supplied in the form of punched output cards which are used in later analysis steps. Additionally, the statistics function will produce training class histograms in user-designated channels. These histograms serve as a partial check as to whether each training classes' data is Gaussian (unimodal) in nature. Serious departure from a Gaussian distribution may necessitate refinement of the training class data.

Feature selection. The feature selection program assists the analyst in finding the middle ground between greater classification accuracy and increased computer time. The program calculates the statistical distance in N-dimensional space (N=# of channels) between the training classes provided. The requested channel combinations are then ranked in terms of the average or the minimum pairwise distance between all pairs of classes. If the statistical distance between significant spectral class pairs is low, it may be necessary to repeat some of the previous analysis steps.

Classification. Classification of the unknown data is the last step in the analysis sequence and represents the culmination of all previous analyses. Program inputs include the statistics deck, the selected combination of channels, and coordinates of the area to be classified. The pattern recognition algorithm, as applied in this study, individually classifies each pixel into one of the statistically defined training classes on a maximum likelihood basis. The output of

the classification function, combined with a printresults program, results in a classification map with alphanumeric symbols representing the designated spectral classes.

An option that must be considered prior to actual generation of classification maps is thresholding. If this option is not applied, the classification algorithm will classify every data point into the class it most nearly resembles, even though the resemblance may be quite remote. Thresholding allows the researcher to arbitrarily screen out those picture elements not demonstrating a high degree of correlation with user-designated spectr- classes. Thresholded points then appear as blank spaces on the final classification map.

Results and Discussion

August 30, 1973

The initial analysis step obtained gray scale printouts of the study area in all four ERTS-1 channels. These printouts were then compared with black and white, color and color IR aerial imagery of the swamp. Pictureprints of the data in channels 1 and 2, 0.5 - 0.6 μm and 0.6 - 0.7 μm respectively, produced the best delineation of swamp boundaries with the Suffolk scarp on the swamp's western edge being clearly defined. In addition, U.S. route 460 and the Norfolk and Western railway were discernable cutting east to west across the northern region of the swamp. Pictureprints produced of channels 3 and 4, 0-7 - 0.8 μm and 0.8 - 1.1 μm respectively, were especially useful in the delineation of water, due to its high absorbancy in these wavelengths. Lake Drummond, located in the swamp's center was clearly differentiated from the surrounding forest, however, none of the numerous drainage ditches located in the swamp could be identified. This is believed to be due to tree overhang and the characteristic low water levels of the swamp in August.

In order to determine the distribution of spectral information taken over the swamp, the clustering algorithm was run on eleven training fields (15,894 data points). Cluster results maps were then printed which contained alphanumeric symbols indicating the geographic location of spectrally similar materials. Clustering performed with all four wavelength channels was not found to be optimal for obtaining spectral separability within the forested training area. Comparison of the cluster means and standard deviation values in all four channels revealed the reason for this less than optimal

cluster separability. Within channels 1 and 2 the cluster radiance means were nearly identical, thereby causing a large amount of data overlap in two of the four clustering space dimensions.

Through elimination of channels 1 and 2 in the clustering process, the number of separable clusters was increased. This is illustrated by comparing the separability quotient values for a four channel cluster run versus a two IR channel cluster run. A value of 0.75 is often used as the breakthrough point for cluster separability. Upon examination of a "maxclas (12)" cluster run, it was determined that fifteen of the separability quotient values were less than 0.75. However, one value of less than 0.75 resulted from two IR channel clustering.

Further analysis of the two IR channel clustering suggested the presence of approximately thirteen spectral groups which were provided to the statistics processor. In addition to calculating the mean vector and covariance matrix for each of the thirteen forest classes, the statistics processor was requested to graph histograms of each training class in all four channels. These histograms were printed so that the distribution of spectral data within each class could be examined. It was found that each class was distributed in an approximate Gaussian manner in all four channels. The statistics processor also produced a coincident spectral plot, which illustrated the relative amplitude of each classes' spectral response in each of the four ERTS-1 channels. Generally, channels 1 and 2 were incapable of differentiating one forest class from another. This was because the class radiance value distributions overlapped one another in these two channels. Channels 3 and 4, on the other hand, contained a wider range of mean spectral values and, therefore, demonstrated the ability to distinguish between the thirteen forest spectral classes.

The next step of the analysis, feature selection, was used to determine the combination of available channels that would yield the most accurate classification results with a minimum amount of computer time. The statistical figure of merit calculated by this function is transformed divergence (Swain 1973). It is a "measure of the dissimilarity of two distributions" and "provides an indirect measure of the ability of the classifer to discriminate successfully between them". The strategy utilized was to weight all classes equally and maximize the pairwise transformed divergences.

Table I gives a summary of three computer experiments.

TABLE I

ERTS CHANNELS USED	TRANSFORMED DIVERGENCE AVERAGE	MINIMUM
1, 2, 3, 4	1960	1204
3, 4	1954	1169
1, 2	432	18

Even though the final classification used all four ERTS bands, clearly the IR bands alone would produce essentially the same classification. Once again, the redundant information content of channels 1 and 2 clearly indicate failure for spectral classification schemes based wholly on these bands for this application.

In the last step of the analysis sequence, the classification algorithm, in conjunction with the printresults function, generated a map-like display. Each spectral class was depicted by a user-defined alphanumeric symbol. These symbols were changed throughout the study in an attempt to bring about easier visual pattern detection. Overall training field classification performance was 96.0%; a figure that indicates the pattern recognition algorithm encountered very little confusion in the mapping of training field data. Application of an arbitrary threshold value (2.0) easily differentiated materials dissimilar to the mapped forest classes. Lake Drummond, located in the swamp's interior, was correctly thresholded, as well as US route 460 and agricultural fields which delimit the swamp on the east, west and south.

Subsequent analysis of the classification map necessarily centered upon determination of the correspondence between spectrally similar ground cover (the map symbols) and categories of informational value, e.g., deciduous or coniferous forest, stand density, etc. Spectral class thirteen, exhibiting the most absorbent qualities of the mapped spectral classes, corresponded closely with dense, monospecific stands of Atlantic white cedar (Chamaecyparis thyoides). Misclassifications did occur, however, and these were observed primarily in two different areas. Several solitary incorrect mappings were noted around the shores of Lake Drummond, a phenomena which can be attributed to pixel

averaging the reflectance of water and forested terrain. Misclassifications also occurred within agricultural fields adjacent to the swamp. These incorrect mappings may be due to the presence of standing water in the fields at the time of satellite data acquisition. Spectral class twelve most closely corresponded to forest stands dominated by Atlantic white cedar, but interspersed with a mixture of hardwoods (mostly Red maple, Acer rubrum, and Sweet gum, Liquidambar styraciflua). By mapping the combination of spectral classes twelve and thirteen, a good representation of Atlantic white cedar present in the swamp has been attained. (See Figure 2).

Further research concerning correspondence between the remaining eleven spectral classes and actual forest cover is progressing, though some problems have been encountered. Unlike the Atlantic white cedar stands which occur as monospecific communities, other plant communities within the swamp are characterized by the presence of several tree and/or shrub species. This leads to a situation of complexity and natural randomness that makes classification into meaningful categories difficult. Problems have also been encountered in attempting to locate, with any degree of certainty, the position of specific forested areas in the ERTS digital data. This is primarily due to: (1) the northeast-southwest skew contained in ERTS-1 MSS data; (2) a lack of large, identifiable land features within the swamp (except Lake Drummond); (3) rectangular computer output format. These problems have been solved to a degree, in that locations in the ground scene can now be generated by an affine mapping transformation developed by Blais (1975).

Another difficulty inherent in mapping diverse vegetation with low resolution scanner data includes pixel averaging. Because tree and shrub species that comprise the swamp's plant communities are much smaller than the 80 meter square pixel size, and are unevenly distributed, spectral characteristics recorded by the scanner will not always be an accurate indicator of a specific species composition. Hypothetically, at certain times of the year, a pixel containing a mixture of 25% Loblolly pine (Pinus taeda), and 75% Red maple may have average reflectance characteristics identical to a pixel averaging the reflectances of 50% Yellow poplar (Liriodendron tulipifera), and 50% Sweet gum. Of course, temporal scanner data obtained during subsequent seasons of the year may remove this spectral signature ambiguity. Heller (1973), using photogrammetric techniques, reported

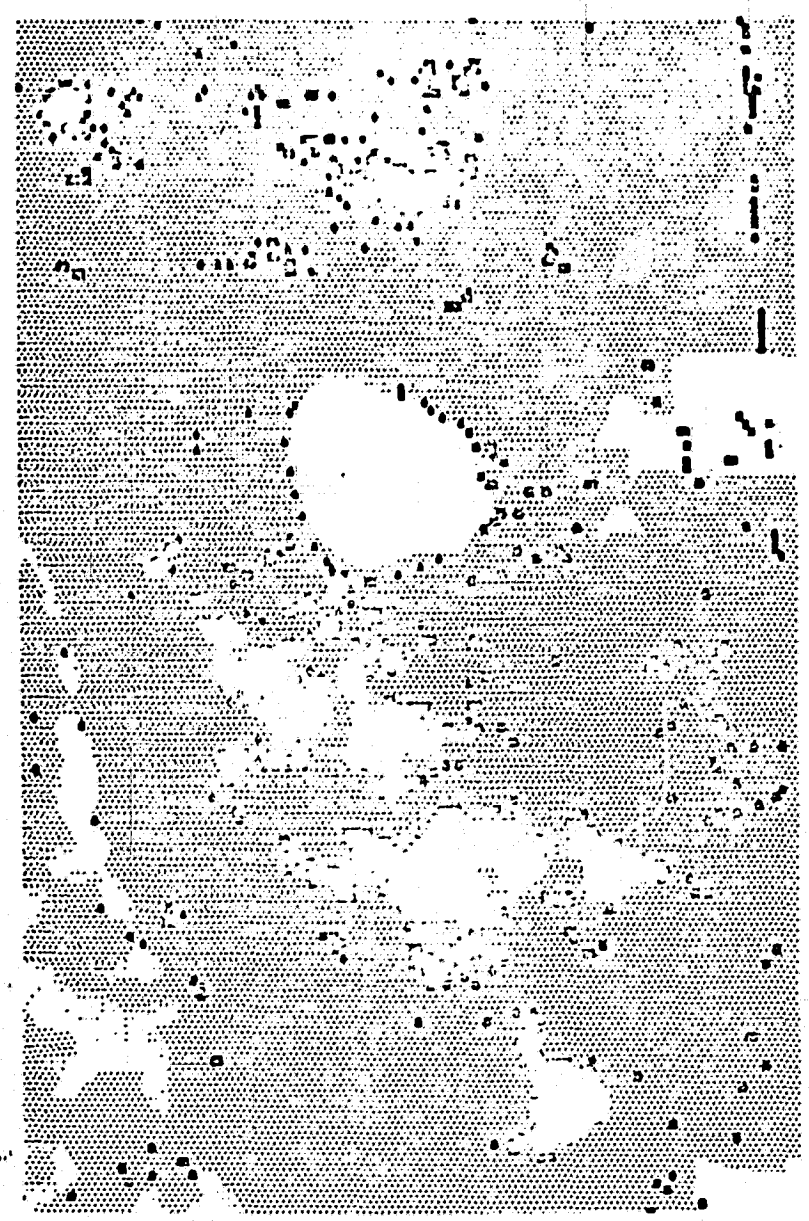

Fig. 2 Classification map of the Great Dismal Swamp (dark regions indicate Atlantic white cedar, thresholed pixels occur as blank areas). Lake Drummond is the central oval feature. North is towards the top.

that forest discrimination with ERTS-1 data was poorest during the summer months (the season during which this study's data was taken) and yielded the best results during spring, fall, and winter). This lends support to the idea that accurate classification of the swamp's vegetational communities will require analysis of data acquired during two or more seasons of the year.

Seasonal Analysis (Aug. 30, 1973 and Oct. 10, 1972)

Even though ERTS is in a sun-synchronous orbit, illumination of the ground scene does change seasonally due to motion of the sun on the ecliptic and variations in the sun-earth distance. Moreover, the spectral reflectivities of different ground features change with many variables, i.e., temperature, moisture content, time in growing season, meterological visibility, etc. Additionally, since the solar elevation angle changes, the scattering angle changes. All of these factors contribute to changes in scene-to-scene radiance values of any one ground feature.

As a first attempt at modeling this complex phenomena, it was deemed desirable to calculate the undepleted insolation at image time. Using the method described by Smart (1965) a computer program was written to provide the undepleted insolation (top of atmosphere) for any location on the earth as a function of time in a year at image time for the ERTS passes. Additionally, the total daily insolation curve for each location is provided. Figure three gives these results for the Dismal Swamp at 1515 GMT as a function of days past perihelian passage (Jan. 4, 1973). The Aug. 30, 1973 date is noted.

Since ERTS MSS sensors have sensibly square response functions over their active spectral range, the signals obtained by each band for a white viewing scene is then just the integral of the solar black body over the response function. Assuming a 5750K solar black body, this integration of the Planck function leads to the values listed in Table II for the energy flux in each sensor.

Table II

Band	Wavelength Microns	% of a 5750°K Black Body	Maximum Radiance MW/cm^2-SR
	.5 - .6	12.9	2.48
	.6 - .7	11.4	2.00
	.7 - .8	9.5	1.76
	.8 - 1.1	18.5	4.60

The field of view is constant for all sensors, and thus the signal outputs for a viewing surface whose albedo is one (total reflection) will fall into those ratios.

In an attempt to determine seasonal fluctuations of LARS statistics, two ERTS images were examined (August 30, 1973 frame number 1403-15132 and October 10, 1972 frame number 1079-1514). Identical training fields were used and the radiance means and standard deviations were generated for six forest spectral classes for those two dates. Table III gives the means for each date, band, and class, as well as the average over classes of the standard deviations for each band.

Table III
Forest Spectral Class Statistics

	Aug 20, 1973				Oct 10, 1972			
	Band							
Class	1	2	3	4	1	2	3	4
1	26.61	15.91	43.43	25.78	19.83	10.91	35.04	22.48
2	26.14	15.44	42.33	24.09	18.98	10.98	33.32	20.72
3	26.06	15.17	41.06	24.14	19.69	10.71	31.54	21.37
4	26.13	15.61	38.94	22.50	19.87	11.06	30.50	19.41
5	26.46	15.60	40.18	23.00	19.42	10.88	28.88	18.26
6	26.47	16.91	37.62	21.12	19.21	10.82	26.29	16.94
$\langle\sigma\rangle$	0.23	0.61	2.15	1.58	0.36	0.12	3.13	2.06

Seasonal differences are traceable to many variables. A major difference for scenes imaged on different dates is the solar illumination. The ratio of the undepleted insolation at image times for the two dates was determined to be (i = August 30, 1973; j = October 10, 1972).

$$\frac{Ii}{Ij} = 1.244 \qquad \text{(eq. 1)}$$

This is also the ratio of the cosines of the solar elevation angles at image time. Calculation of percent differences of

the forest class means at the two dates to the insolation ratio, yields a first estimate of class changes between image time. Table IV lists this ratio

$$(((\mu_i/\mu_j) - 1.244)/1.244) \times 100 \qquad \text{(eq. 2)}$$

for each class and band. If this percentage is positive, the August 30 image is brighter than the insolation corrected October 10 image.

Table IV
Per Cent Difference

Class	Band 1	2	3	4
1	+7.8	+17.2	-0.4	-7.8
2	10.7	13.0	+2.1	-6.54
3	6.4	13.9	4.6	-9.2
4	5.71	13.4	2.6	-6.8
5	9.5	15.3	11.8	+1.3
6	10.7	25.6	15.0	+0.65

In order to estimate the magnitude of seasonal differences, a knowledge of some environmental parameters is required (see Table V). Meteorological data is from Norfolk Regional Airport located about 25 km NE of the training fields. The optical depth, τ, is calculated from the work of Potter and Shelton (1974) for the known visibility. The precipitable water layer is deduced from radiosonde and the TSTSP (Total sun target satellite path water amount) is determined in the method of Pitts, McAllum and Dillinger (1974).

Table V
Environmental Parameters

	Oct. 10, 1972	Aug. 30, 1973
Optical Depth (0.5 μ)	0.30	.49
Dew Point (°C)	5	25
Temperature (°C)	13.9	31.1
Absolute Humidity (gm/m^3)	6.6	22.6
Visibility (km)	24.1	1.6Fog
Percipitable water layer (cm)	2.0	5.8
Coefficient of Haze (cohs)	0.6	
Wind azimuth (°)	10	10
Speed (knts)	15	4
Solar Elevation	40°	52°
TSTSP (cm)	5.11	13.2

J. Messmore, G. E. Copeland, and G. F. Levy

Effects of Haze

Potter and Shelton have done a study on the effects of atmospheric haze and varying sun angles on the LARS classification accuracy for corn and soybeans. Since both Raleigh and Mie scattering are inversely proportional to the fourth power of wavelengths, it is to be expected that for fixed solar angles, the scattering activity of atmospheric haze will increase the radiance of ERTS scenes most in MSS band 4 and least in MSS 7. Examination of their results for optical depth with meteorological visibility, yields a value of $\tau = 0.3$ for October 10, 1972. Calculation of τ for August 30, 1973 from visibility is not useful, since a fog bank was adjacent to the airport.

Potter and Shelton give tabular results for the variation of class means μ, with optical depth, τ, for corn and soybeans for each ERTS band. Fitting their results in a least squares linear regression yields

$$\mu \text{ (corn)} = 17.86\ \tau + 22.18$$

$$\mu \text{ (soybeans)} = 17.35\ \tau + 23.30 \qquad \text{(Eq. 3)}$$

over the range $\tau = 0$ to 0.4. If we assume that the average of the slopes (17.51) is appropriate for our forest classes, and using $\tau = 0.3$ for the October 10 optical depth, then the haze free values of the October 10 class means is given by (MSS 4)

$$\mu_j \text{ (haze free)} = \mu_j - 5.25 \text{ (eq. 4)}$$

Correcting for insolation differences, we deduce the August optical depth (MSS 4) to be

$$\tau_i = \frac{\mu_i - 1.244\ \mu_j \text{ (haze free)}}{17.51} \qquad \text{(Eq. 5)}$$

This assumes that the reflectance is constant in time for a given spectral class. Calculations for each class, however, yield almost identical values of τ_i (0.49 ± 0.03). Using an empirical relationship between coefficient of haze (cohs), mass loading, and visibility, indicates τ for this date as 0.5. Similar results are possible for other ERTS bands but the effect is progressively smaller with increasing band number.

Examination of Table IV (MSS 4) for all six forest classes, thus indicates the increased radiance can nearly all be accounted for by an increased optical depth, i.e., aerosol loading. This is quite realistic since: the air is of maritime origin; the relative humidity is high (77%); air temperature is 88°F; and contrast in the MSS 4 imagery is reduced over October imagery.

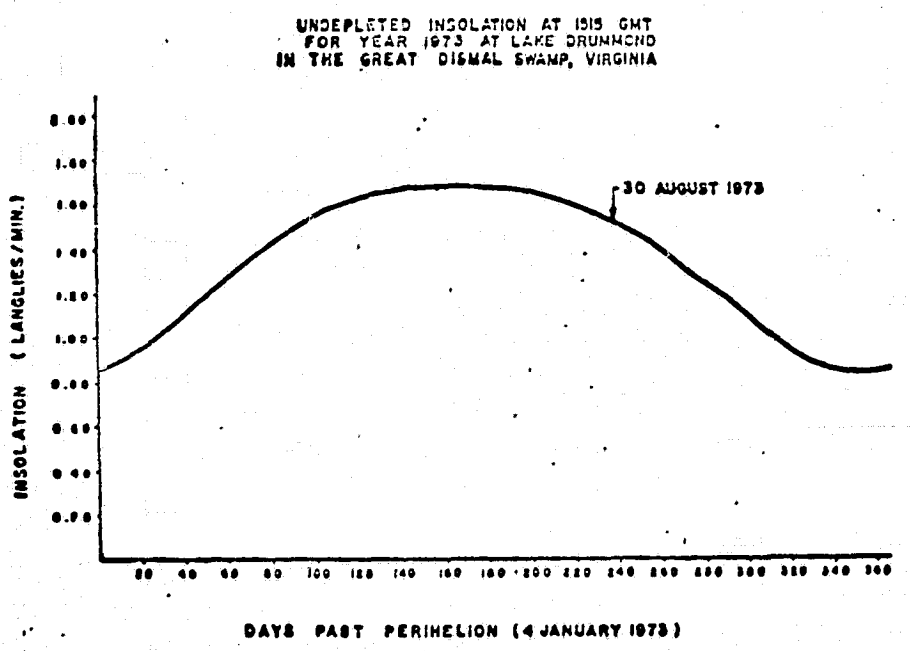

Fig. 3.

Effects of Water Vapor

Pitts, McAllum and Dillinger (1974) have discussed the effects of atmospheric water vapor on the classification accuracy of LARS when used on ERTS data. A major problem exists with MSS 7 (.8 to 1.1 microns), where water absorption bands occur. They calculated the atmospheric transmission function, including 2070 compressed water vapor lines, in a ten layer transmission model normalized to the response function of MSS 7. Using their results of average transmission versus total atmospheric water content percipitable (vertical loading), it is possible to "correct" for water vapor absorption.

Radiosonde data from Wallops Island, Va.; Cape Hatteras, N.C.; and Washington, D.C. were used to calculate the percipitable water load for August 30, 1973. This yielded 5.8 cm in vertical and a transmission of 78%. Since the solar flux traveled a slant path (incoming) as well as a vertical path (outgoing), the total transmission for this date was 64%. No radiosonde soundings were available for October 10, 1972, but a realistic estimate for that date yields a total transmission of 75%.

If one multiplies the insolation ratio by the ratio of total transmission coefficients for those dates, then this may be used to normalize the ratios of mean radiances of training fields for those image dates. For example:

$$\frac{\mu_i}{\mu_j} - \frac{(.64)(1.244)}{.75} \qquad \text{(eq. 6)}$$

Calculations of percent difference for the quantities, yields the data shown in Table VI for water and sun angle corrected radiance ratios of 6 forest spectral classes. Positive values indicate increased reflectance.

Table VI

Water - Sun Angle Corrected Radiance Ratios

Forest spectral Class	1	2	3	4	5	6
Percent Differences	+8.2	+9.7	+6.6	+9.3	18.9	+17.6

Note that all forest classes are brighter in August. Classes 5 and 6 show the largest increase (about 19%) since these areas were logged between image dates.

CONCLUSION

Application of the LARS system in an unsupervised forest classification procedure using ERTS data has indicated that this procedure can successfully identify some plant communities in the Great Dismal Swamp. Forest spectral class means in MSS bands 4 and 5 are of little use in classification of the ground cover since those means are not sufficiently dissimilar. Classification depends almost entirely on analysis of MSS 6, 7. Seasonal changes in forest spectral statistics may be deduced from the effects of

varying sun angle, aerosol loading, and water vapor absorption, if sufficient environmental parameters are available.

Acknowledgements

We would like to thank Drs. R. N. Blais, E. C. Kindle, E. G. Astling, and Mr. T. H. Lerner who supplied technical assistance and analysis of this problem and to the personnel of Wallops Island Chesapeake Data Bank for their assistance in acquisition of aerial imagery of the Great Dismal Swamp. In addition, we would like to express appreciation to Virginia Carter, U.S.G.S., and Phil Renfroe for their assistance in this study. Financial assistance for this work was supplied through NASA grant NGL47-003-067.

References

Blais, R. N., Copeland, G. E., Lerner, T., 1975. Use of LARS System for Quantitative Determination of Smoke Plume Lateral Diffusion Coefficients from ERTS Images of Virginia, Fourth Annual Remote Sensing of Earth Resources Conference, University of Tennessee Space Institute.

Carter, V. 1974. The Dismal Swamp: Remote sensing applications. U.S. Geological Survey, National Center. 19 pp.

Erb, R. B. 1973. The Utility of ERTS-1 data for applications in agriculture and forestry. pp. 75-85. In Proc. of Third Earth Res. Tech. Satellite-1 Symposium. Vol. 1 NASA SP-351. U.S. Govt. Printing Ofc. Washington, D.C.

Heath, G. R. and H. D. Parker 1973. Forest and range mapping in the Houston area with ERTS-1. pp. 167-172. In Proc. Symp. on Significant Results obtained from ERTS-1. Vol. 1, NASA SP-327. U.S. Govt. Printing Ofc. Washington, D.C.

Heller, R. C. 1973. Analysis of ERTS imagery-problems and promises for foresters. In Proceedings Symposium IUFRO. Freiburg, Germany: 373-393.

Lindenlaub, J. C. 1972. Remote sensing analysis: a basic preparation. LARS information note 110471. The laboratory for applications of remote sensing. Purdue University. 90 pp.

Meanley, B. 1973. The great dismal swamp. Audubon naturalist society of the central Atlantic states, Inc. 48 pp.

Pitts, D. E., McAllum, W. E., and Dillinger, A. E. 1974. The Effect of Atmospheric Water Vapor on Automatic Classification of ERTS Data. Proceedings of the 9th International Symposium on Remote Sensing of Environment, p. 483.

Potter, J. and Shelton, M. 1974. Effect of atmospheric haze and Sun Angle on Automatic Classification of ERTS-1 Data. Proceedings of the 9th International Symposium on Remote Sensing of Environment. p. 865.

Smart, W. M. 1965. Textbook on Spherical Astronomy, Cambridge Univ. Press.

Swain, Philip H. 1973. Pattern Recognition: A Basis for Remote Sensing Data Analysis. LARS Information Note 111572, Purdue Univ.